Supporting information for

Structural Modulation of TiO_2 Supports by Cr Doping to Tune Ir Electronic Structure and Accelerate Acidic OER

Chen Cao[a,b,c], Shirui Cui[a], Yanqin Li[a], Chunyang Zhao[a], Wei Hu[a], Feng Shi[b,c], Zelong Li [a] *, Yu Tang [a] *

[a]Key Laboratory of Advanced Catalysis, Gansu Province, State Key Laboratory of Applied Organic Chemistry, Key Laboratory of Nonferrous Metal Chemistry and Resources Utilization of Gansu Province, College of Chemistry and Chemical Engineering, Lanzhou University, Lanzhou, Gansu 730000, China

[b]State Key Laboratory of Low Carbon Catalysis and Carbon Dioxide Utilization Lanzhou Institute of Chemical Physics, Chinese Academy of Sciences No.18, Tianshui Middle Road, Lanzhou, 730000, China

[c]University of Chinese Academy of Sciences, Beijing 100049, China

Correspondence: Zelong Li (lizl@lzu.edu.cn); Yu Tang (tangyu@lzu.edu.cn)

Keywords: Oxygen evolution reaction; Proton exchange membrane water electrolysis; Hydrogen production; Electrocatalysis.

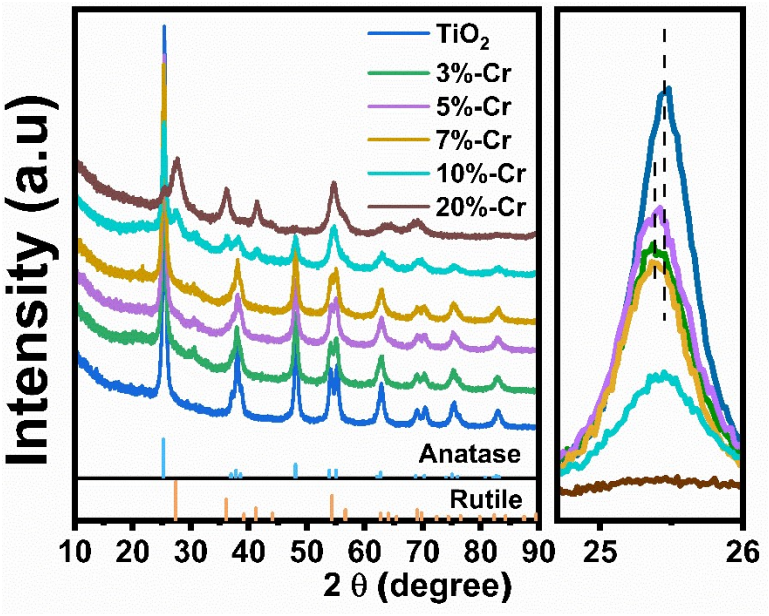

Fig. S1. XRD of catalysts with different contents of Cr.

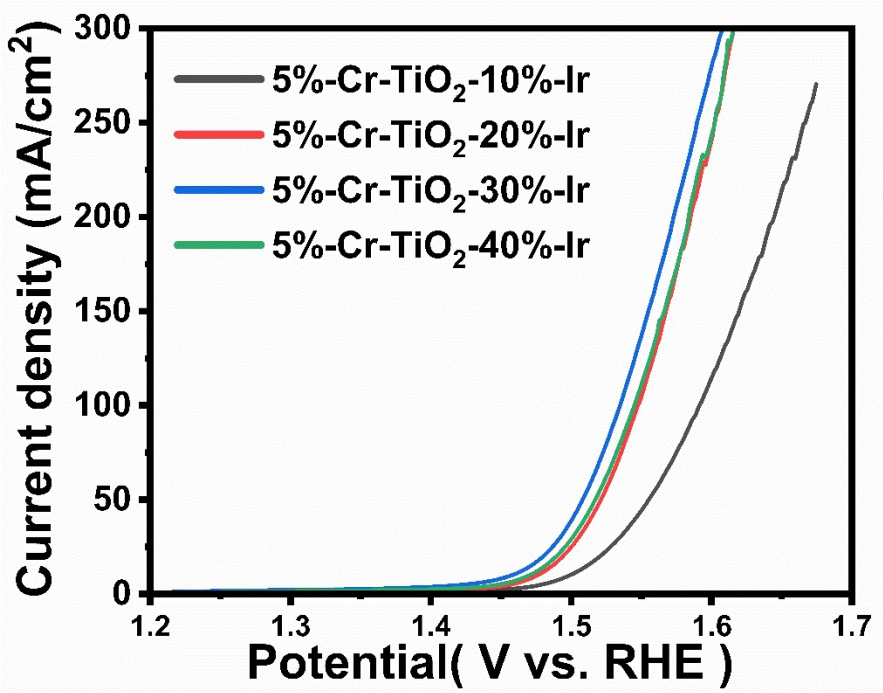

Fig. S2. LSV curves of catalysts with different contents of Ir.

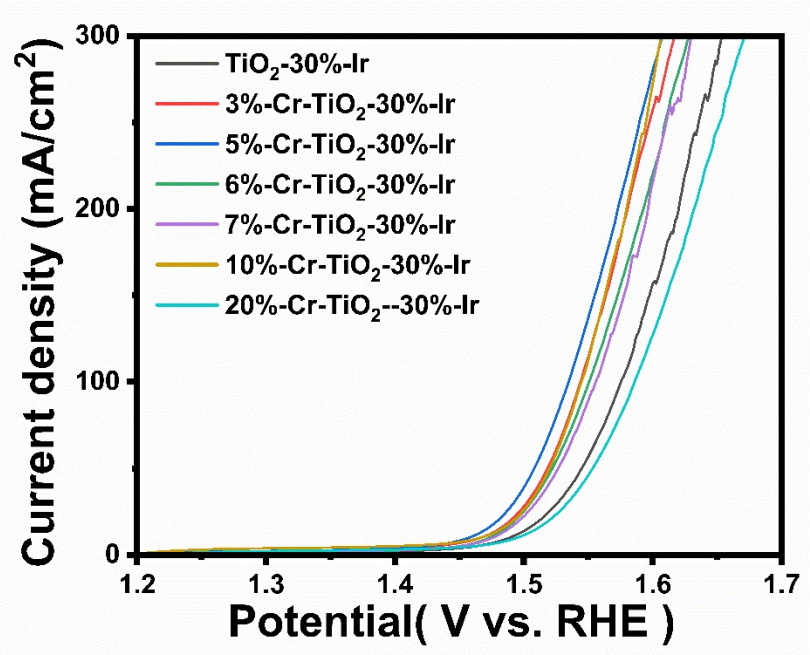

Fig. S3. LSV curves of catalysts with different contents of Cr.

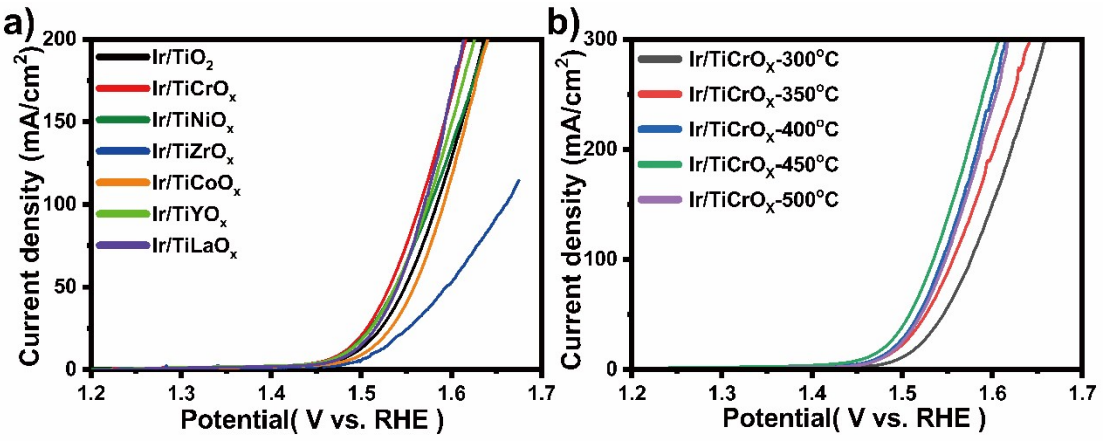

Fig. S4. (a) LSV profiles of catalysts with different elemental doping. (b) LSV profiles of catalysts treated at different heating temperatures.

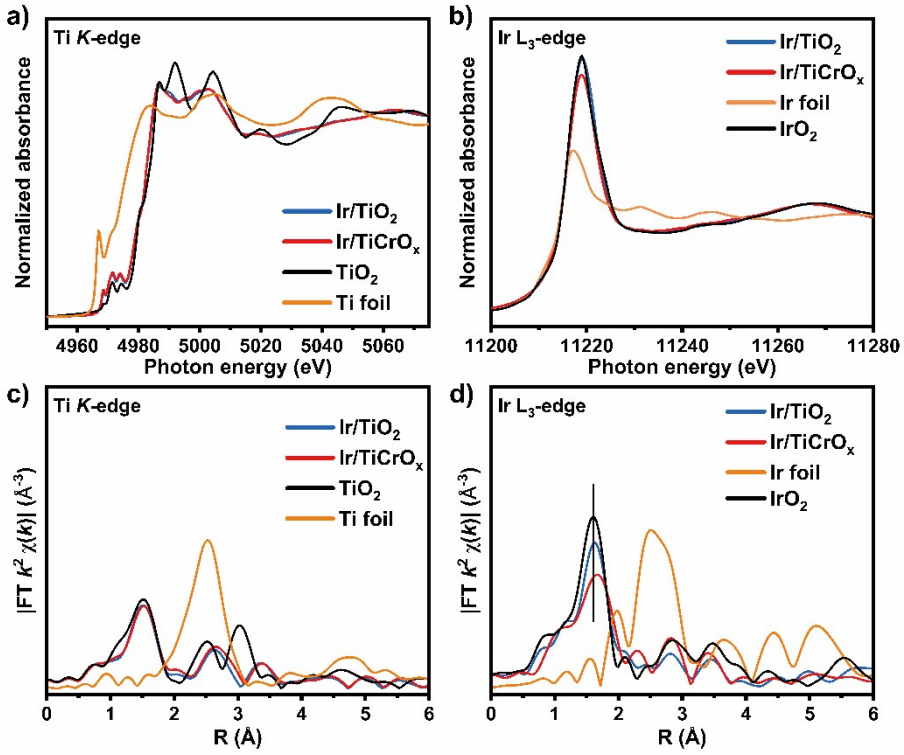

Fig. S5. (a) Ti K-edge and b) Ir L_3-edge XANES spectra of different catalysts. (c) Ti K-edge and (d) Ir L_3-edge FT-EXAFS spectra of different catalysts.

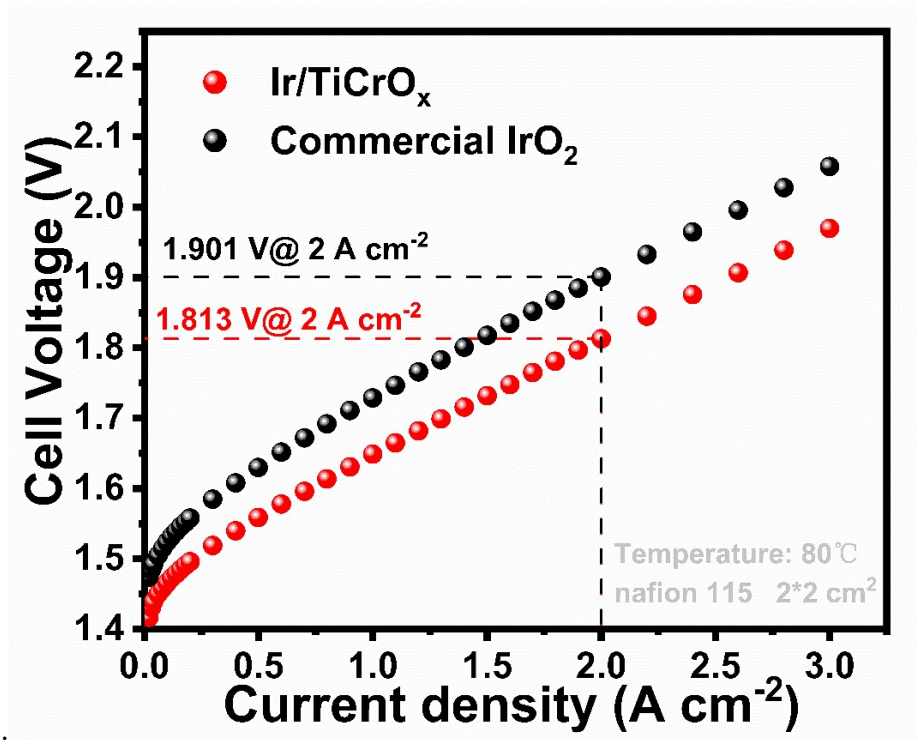

Fig. S6. Steady-state polarization curves of PEMWE using Ir/TiCrO$_x$ and commercial IrO_2 as anode catalysts.

Table S1. Parameters used in EXAFS fittings.

Sample	Shell	Bond length (Å)	Coordination Number	σ^2 (Å^2)	E_0 shift (eV)	R-factor
Ir/TiO$_2$	Ti-O	1.94±0.02	5.8±0.6	0.002±0.001	-	0.020
	Ti-Ti	3.04±0.02	4.0±0.7	0.004±0.002	1.6±2.7	
	Ir-O	2.01±0.01	5.7±0.7	0.005±0.002	2.9±1.2	0.018
	Ir-Ir	3.12±0.04	1.8±0.3	0.009±0.006		
Ir/TiCrO$_x$	Ti-O	1.96±0.01	5.7±0.5	0.004±0.001	4.5±1.6	0.006
	Ti-Ti	3.05±0.03	4.2±0.5	0.009±0.003		
	Ir-O	2.02±0.03	5.3±0.4	0.009±0.005	2.3±2.2	0.019
	Ir-Ir	3.13±0.01	2.1±0.2	0.013±0.002		

[a]. The value of the amplitude reduction factor (S_0^2) was fixed to 0.80; [b]. Bond length is the interactomic distance; [c]. CN is the coordination number; [d]. σ^2 is Debye-Waller factor (a measure of thermal and static disorder in absorber scatter distance); [e]. E_0 shift is edge-energy shift (the difference between the zero kinetic energy value of the sample and that of the theoretical model); [f]. R factor is used to value the goodness of the fitting; * This value was fixed during EXAFS fitting, based on the known structure of Ti and Ir.

Table S2. Comparison of various PEMWE operation conditions and catalyst performances.

Catalyst	Anode loading (mg cm^{-2})	Cell activity (V @ A cm^{-2})	Total time	Refs.
$Ir/TiCrO_x$	0.5	1.73 V @ 2 A cm^{-2} 1.60 V @ 1 A cm^{-2}	350 h @ 2 A cm^{-2}	This work
$RIE\text{-}Ir/CeO_x$	0.4	1.62 V @ 2 A cm^{-2}	2000 h @ 1 A cm^{-2}	[1]
IrVI -ado (MnO_2/p-PTL)	0.08	1.77 V @ 2 A cm^{-2}	2500 h @ 1.8 A cm^{-2}	[2]
Ir/Ti_3O	0.3	1.77 V @ 2 A cm^{-2}	700 h @ 1 A cm^{-2}	[3]
Ir/TiO_x@Ti	0.3	1.77 V @ 2 A cm^{-2}	400 h @ 2 A cm^{-2}	[4]
$IrO_2(101)$	1.5	1.78 V @ 2 A cm^{-2}	10000 h @ 1.5 A cm^{-2}	[5]
$Ir@IrO_x/m\text{-}Nb\text{-}TiO_2$	0.27	1.72 V @ 2 A cm^{-2}	3000 h @ 2 A cm^{-2}	[6]
LaIr-Co3O4	0.2	1.61 V @ 1 A cm^{-2}	1000 h @ 1 A cm^{-2}	[7]
Ir/TiN	0.1	1.80 V @ 2A cm^{-2}	500 h @ 1 A cm^{-2}	[8]
DA_IrOx/TiO_2	0.3	1.82 V @ 3A cm^{-2}	100 h @ 2 A cm^{-2}	[9]
$Ir\text{-}LiCoO_2$	0.5	1.64 V @ 1 A cm^{-2}	150 h @ 1 A cm^{-2}	[10]

References

[1] Shi W, Shen T, Xing C, et al. Ultrastable supported oxygen evolution electrocatalyst formed by ripening-induced embedding [J]. Science, 2025, 387(6735): 791-6.

[2] Li A, Kong S, Adachi K, et al. Atomically dispersed hexavalent iridium oxide from MnO_2 reduction for oxygen evolution catalysis [J]. Science, 2024, 384(6696): 666-70.

[3] Zhang K, Zhang L, Zhao Z, et al. Electride-Stabilized Iridium Nanoparticles with Subsurface Oxygen Confinement for Oxygen Evolution Electrocatalysis [J]. Journal of the American Chemical Society, 2026, ASAP.

[4] Zhang K, Liang X, Wang Y, et al. Support-tuned iridium reconstruction with crystalline phase dominating acidic oxygen evolution [J]. Nature Communications, 2025, 16(1): 4567.

[5] Yang D, Zhang C, Qin Y, et al. Single-faceted IrO_2 monolayer enabling high-performing proton exchange membrane water electrolysis beyond 10,000 h stability at 1.5 A cm^{-2} [J]. Nature Communications, 2025, 16(1), 10598.

[6] Ni J, Shi Z, Bai J, et al. Heterointerface Anchored Ir with Localized Strong Orbital Coupling for Durable Proton Exchange Membrane Water Electrolysis [J]. Angewandte Chemie International Edition, 2025, 64(37): e202507896.

[7] Wei Z, Ding Y, Shi W, et al. Lanthanum-assisted lattice anchoring of iridium in Co_3O_4 for efficient oxygen evolution reaction in low-iridium water electrolysis [J]. Nature Communications, 2025, 16(1): 3456.

[8] Lin H Y, Li W J, Lin M Y, et al. Leaching-Induced Ti Trapping Stabilizes Amorphous IrO_x for Proton Exchange Membrane Water Electrolysis [J]. Angewandte Chemie International Edition, 2025, 64(49): e202509888.

[9] Kang J, Wang X, Möhle S, et al. Synthesis, Molecular Structure, and Water Electrolysis Performance of TiO_2-Supported Raney-IrO_x Nanoparticles for the Acidic Oxygen Evolution Reaction [J]. ACS Catalysis, 2025: 5435-46.

[10] Zhao S, Hung S-F, Wang Y, et al. Dynamic Deprotonation Enhancement Triggered by Accelerated Electrochemical Delithiation Reconstruction during Acidic Water Oxidation [J]. Journal of the American Chemical Society, 2025, 147(9): 7993-8003.